CHAPTER 1

INTRODUCTION

On the 26 December 2004 the Mw 9.3 Sumatra-Andaman Earthquake occurred at 00:58:53.4 UTC off the west coast of Northern Sumatra, Indonesia; resulting in about 1,600 km rupture along the fault boundary between the Indian-Australian Plate and the southeastern part of the Eurasian Plate with fault slip of up to 15 m near Banda Aceh (Lay et al., 2004). The massive earthquake triggered a series of devastating tsunamis along the coastline of the Indian Ocean, killing a large number of people and inundating coastal communities across the South and Southeast Asia, including parts of Indonesia, Sri Lanka, India, and Thailand. More than 283,100 people were killed, 14,100 missing and 1,126,900 displaced (USGS, 2005) and a large number of infrastructures were wiped off.

There are a series of faults in southern Thailand, mainly the Ranong and Khlong Marui Fault Zones, which were identified as dormant by the Department of Mineral Resources, Thailand (DMR). However, there was concern among people and responsible government agencies that the 26 December 2004 Earthquake might have resulted in the (re)activation of these faults with consequent earthquakes, which then might have effects to the infrastructure and the people in Southern Thailand.

In order to meet these concerns, the Geophysics Research Group in the Department of Physics at the Faculty of Science, Prince of Songkla University, established in collaboration with the Department of Mineral Resources a seismic network in Southern Thailand. The aim was to monitor possible earthquakes along the Ranong and Khlong Marui Fault Zones, as the Group is equipped with short-period seismometers.

1.1 Review of Literature

1.1.1 The 26 December 2004 Earthquake

The Mw 9.3 earthquake on 26 December 2004 occurred at 00:58:53.4 (UTC time) with an epicenter at latitude 3.925˚ N and longitude 95.982˚ E at a depth of 30 km, on the west coast of Northern Sumatra Island, Indonesia (USGS, 2005; Figure 1.1). The earthquake occurred at the interface between the Indian-Australian Plate and the Burma Plate, as part of the Eurasian Plate, and it was caused by the stress released from Indian Plate subducting under the Burma Plate. This earthquake is the highest magnitude earthquake recorded since the general use of modern digital seismometers worldwide (USGS, 2005)

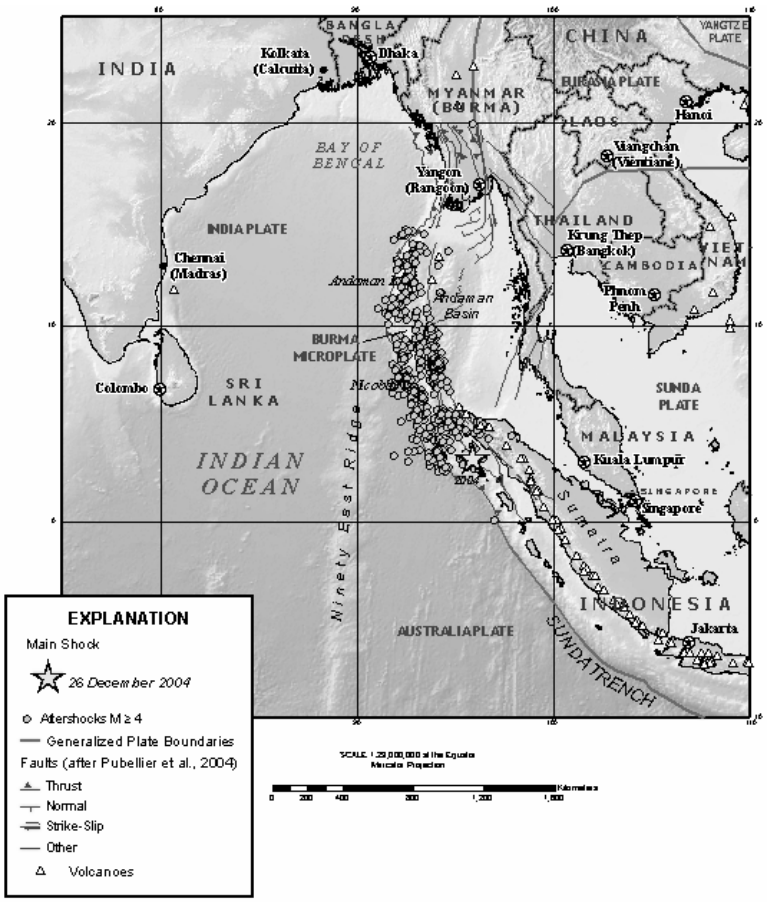

Figure 1.1. The Mw 9.3 Earthquake on 26 December 2004 at 00:58:53.4 (UTC time) at 30 km depth occurred on the west coast of Northern Sumatra Island, Indonesia (USGS, 2005).

Effects of the 26 December 2004 Earthquake

The earthquake on the 26 December 2004, which occurred at the Sunda Subduction Zone, resulted in an uplift of the ocean bottom, which then triggered a number of tsunamis. They subsequently spread throughout the Indian Ocean, affecting the coastlines with losses of life and destruction of a large numbers of onshore structures (USGS, 2005).

Further, data from 60 permanent Global Positioning System (GPS) sites in Southeast Asia recorded crustal deformation during (co-seismically) and after (post-seismically) the 26 December 2004 Earthquake (Vigny et al., 2005). Even GPS stations on the Diego Garcia Island in the Indian Ocean and stations in the Philippines show co-seismic displacement (Figure 1.2).

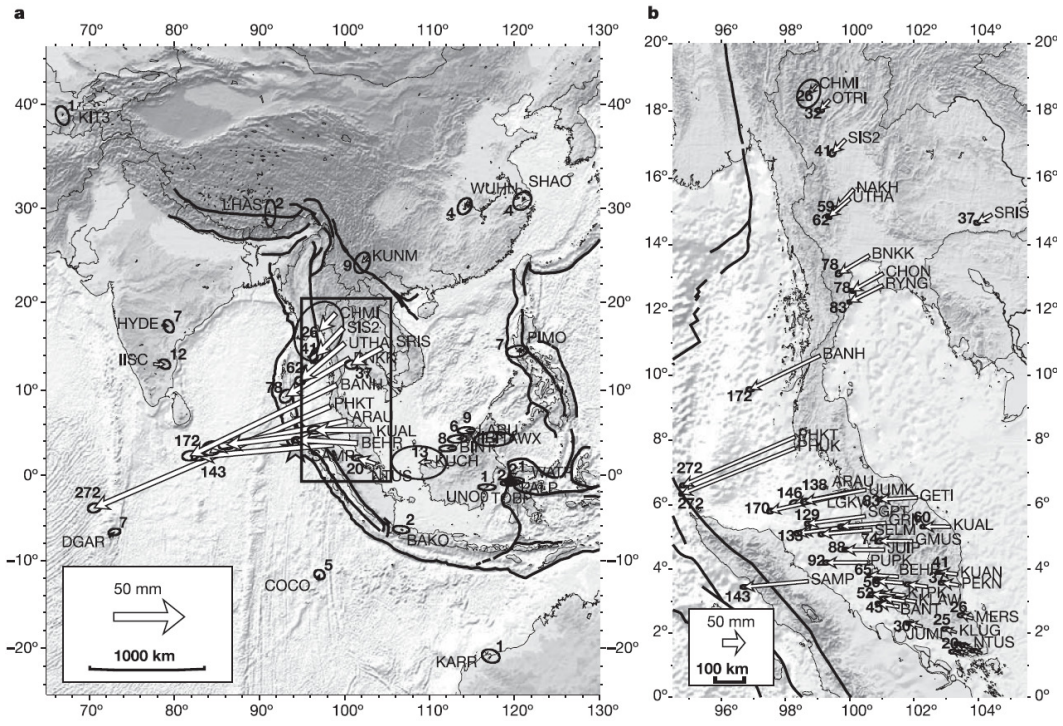

Figure 1.2. Co-seismic displacements from GPS observations. Bold numbers show displacement in mm: (a) overview of Southeast Asia, and (b) a more detailed view of the Thai-Malaysian Peninsula (Vigny et al., 2005).

For stations in Thailand, Malaysia and Indonesia following co-seimic displacements were recorded: 26 cm for Phuket, which was greater than any other

station in Thailand, 8 cm in Bangkok, 3 cm in Chiang Mai, Thailand, 17 cm on Langkawi Island, Malaysia, and 15 cm in Sampali, Indonesia, see Figure 1.2. During a period of fifty days after the earthquake, post-seismically, Phuket Island moved about 34 cm to the South-West direction (Vigny et al., 2005).

After the 26 December 2004 Earthquake, an increasing number of sinkholes were reported in Southern Thailand (DMR, 2005). Sinkholes are a natural phenomena and quite common in southern part of Thailand due to the limestone and evaporate formations. The water dissolves the limestone and transports it away resulting in subsurface holes. When the roofs of these holes become mechanically unstable, for example during ground shaking, the roofs collapse into the hole making it sinkholes (Luhr, 2004)

Figure 1.3. shows the time and location of sinkholes recorded from June 1995 to June 2005 (DMR. 2005). The sinkholes that occurred before the 26 December 2004 Earthquake are shown in close triangle symbol and the sinkholes that occurred after the 26 December 2004 are shown in star symbol.

News reports often associated the occurrence of these sinkholes with the earthquakes in the Sumatra-Andaman region, like on 8 June 2005. Following was reported by the Thai News Agency (TNA): "*The latest earthquake to hit the Indonesian island of Sumatra recently [28 March 2005, noted] has caused massive earth craters to appear in Thailand's southern province of Trang, Provincial Governor Naret Jitsucharitwong confirmed today. Several houses in Wang Wiset district reported cracks today, while officials from the Department of Mineral Resources have discovered four-metre deep soil craters. The limestone soil of the area is particularly prone to earthquake-related subsidence, as limestone is characterized by air bubbles under the soil.*"

Further, on 20 January 2005 The Nation newspaper reported, that a steady stream of air bubbles surfacing 500 meters offshore in Laem Son Bay were observed, discernible for about 10 days. The Department of Mineral Resources and local officials detected a 7 cm wide crack in the ocean floor about 1 km long, which releases the air bubbles. The Ranong Fault Zone, which has been inactive for years,

straddled the area where the ocean floor appeared to have split open. “It becomes active again and releases the bubbles” The Director of the Provincial Geological Office suggested that the earthquake reactivated the dormant Ranong fault with the release of bubbles.

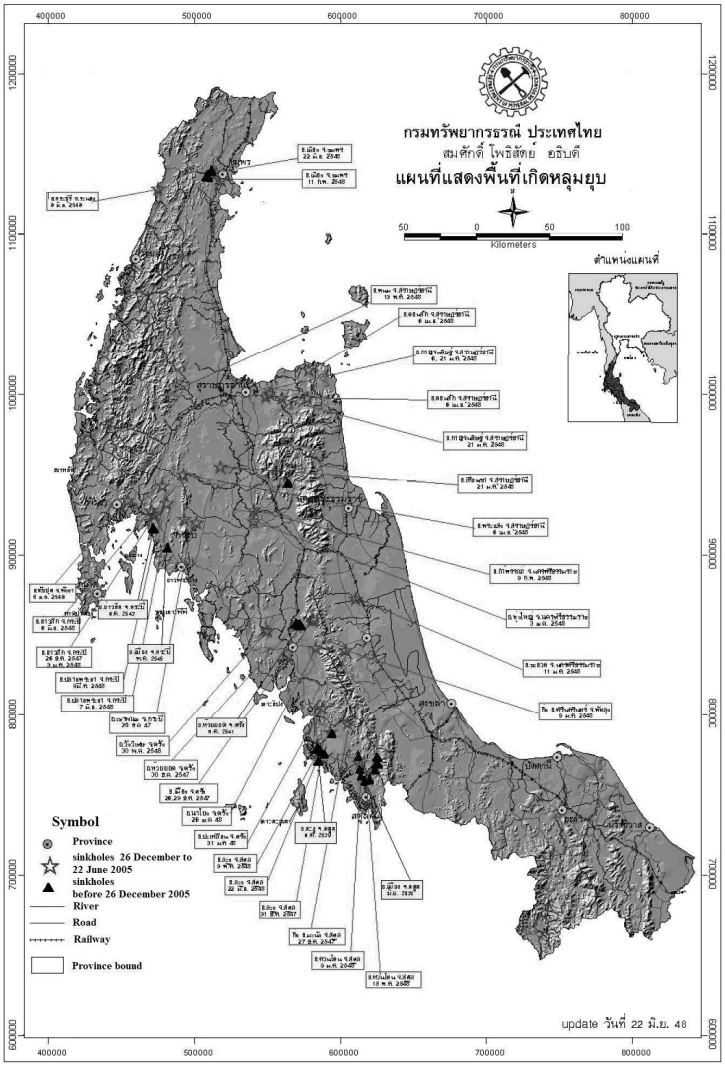

Figure1.3. Time and location of sinkholes in the southern part of Thailand from June 1995 to June 2005. Close triangle show the sinkholes that occurred before the 26 December 2004 Earthquake, and the sinkholes that occurred after the 26 December 2004 are shown in star symbol (DMR, 2005).

1.1.2 Geology and tectonic of Andaman Sea and Thai Peninsula

The Andaman Sea covers an area with a length of 1200 km, from the Arawadi River to the northern part of Sumatra Island and the Malaka Strait, and with a width of 650 km, from the west of the Thai peninsula to Andaman and Nicobar Islands. Since about 32 Ma ago, the Andaman Sea was an active extensional backarc basin east of the Sunda Subduction Zone. The backarc extension, which is normal to N-S striking subduction zone, is combined with strike-slip faulting of the Burma Plate (Curray, 2005, see Figure 1.4.).

The Thai peninsula is a narrow strip of land connected with the Malay Peninsula. The geology and stratigraphy of Thai peninsula are described for the first time in Brown et al. (1951) which provided information on Odovician limestone at Thung-Song, Phuket series in Phuket and the Tertiary Krabi series in Krabi. The fossiliferous Cambrian rocks were reported on Tarutao Island (Buravas, 1961).

Garson and Mitchell (1975) described the five confined basins of tertiary rocks encompassing conglomerate, soft red bed, gray sandstone, sandy shell, clay, limestone, and coal which are located with patchiness on the Pre-tertiary rock on Thai peninsula.

Fault Zones in Southern Thailand

Thailand is part of a geological entity extending from the Chinese province of Yunnan and Shan of Myanmar to the Malay Peninsula in the south. A number of faults are apparent in southern Thailand (Bunopas, 1981), Figure 1.5.

There are two major faults in southern Thailand aligned NE-SW, the Ranong and Klong Marui Fault Zones. Both are presumably converge in the Gulf of Thailand under thick load of late Tertiary sediments within a structural trough to form a single fault, which displaces the Rayong gneissic granites to the Hua Hin area (Garson and Mitchell, 1970).

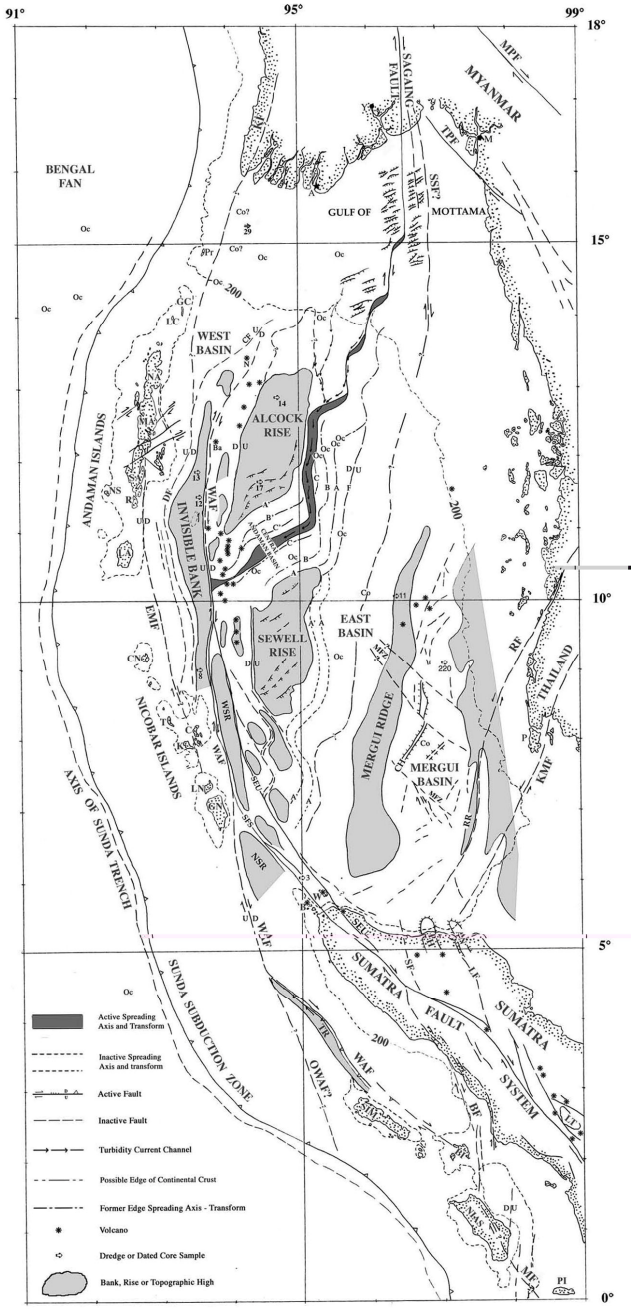

Figure 1.4. Tectonic map of the Andaman Sea area. The Sunda Subduction Zone is where the Indian-Australian Plate subducts under the Eurasian Plate. The major faults align on North-South trench are WAF, OWAF and EMF (the West Andaman Fault, Old West Andaman Fault and Eastern Margin Fault). The fault align on Northeast-Southwest trench are RF and KMF (Ranong Fault and Khlong Marui Fault); from Curray, 2005.

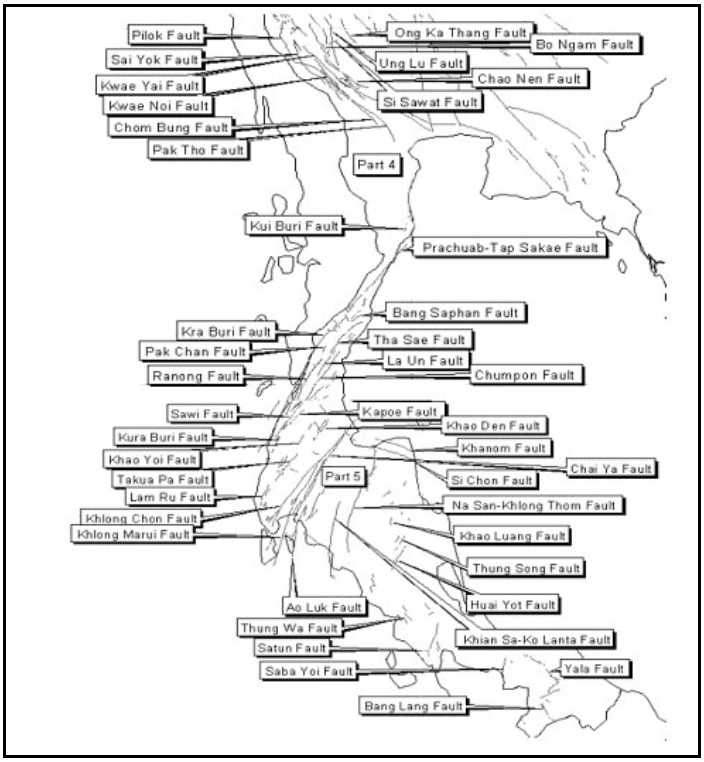

Figure 1.5. Faults in southern Thailand, with location and name (DMR, 1997b).

The Ranong Fault Zone is a strike-slip fault, constituted by a series of faults parallel along NE-SW from the Andaman Sea in Ranong Province to the northeast Gulf of Thailand in Prachuap Khiri Khan and Chumphon Province. The fault lies in the channel of Kra-Buri River, about 270 km in length. The Caborniferous–Permain rocks in the area (Kang–Kra-Chan Group) have been affected by these faults (Garson and Mitchell, 1970). The fault moved 20 km eastward over the period of 113 $\pm$ 8 million years. During the period of Tertiary, the fault zone moved right lateral (Bunopas, 1981; Tapponnier et al., 1986).

The Khlong Marui fault is strike-slip nature, aligned parallel to Ranong Fault Zone. It initially moved 150 km sinistral, and then moved right lateral at the transition of Jurassic and Cretaceous. In the middle of Tertiary, the fault is similar to the Ranong Fault Zone (Tapponnier et al., 1986; see Figure 1.6).

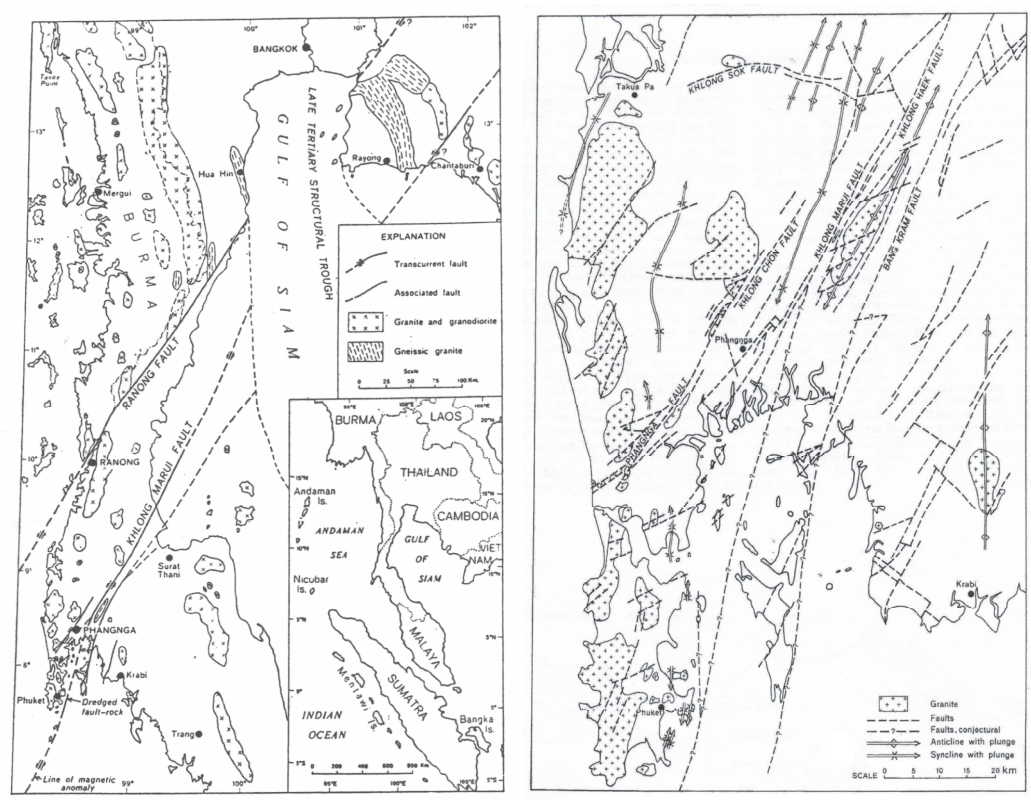

(a) (b)

Figure 1.6. Ranong Fault Zone (a) and Khlong Marui Fault Zone (b) with granitic rocks in Thai Peninsula (Garson and Mitchell, 1970, 1975).

The Khlong Marui and Ranong faults are located at the junction of the Sumatra and Andaman-Nicobar region of Sunda Arc,which occupies the southwestern area of Sunda shelf. The plate tectonic concept and volcanic activity in Sunda Arc are related to the descent of lithosphere that spread in north-eastwardly along inclined Benioff zone (Garson and Mitchell, 1970)

It was postulated, that the lateral displacements along Khlong Marui and Ranong Faults are caused by the lithosphere beneath to the Andaman–Nicobar prior to the existence of Mentawi Island in Jurassic period. Before the Jurassic time the areas of continental crust which was moved to the southeast of its present location about 200 km south-west of its original site (Figure 1.7 (a)). From the late Jurassic to

the early Cretaceous time the occurrence of lithosphere descent to the crustal remains and the expansion of ocean floor have moved north-eastwardly (Figure 1.7 (b)).

The consequence of differential horizontal movement of southern plate, Sumatra; Malaysia; and Sunda shelves, and the northern plate, Thai peninsula and Andaman Basin, have been transformed into faulting along the Khlong Marui and Ranong faults and the margin of Sunda shelf plate has moved to the present location in the early of Cretaceous period (Garson and Mitchell, 1975, Figure 1.7).

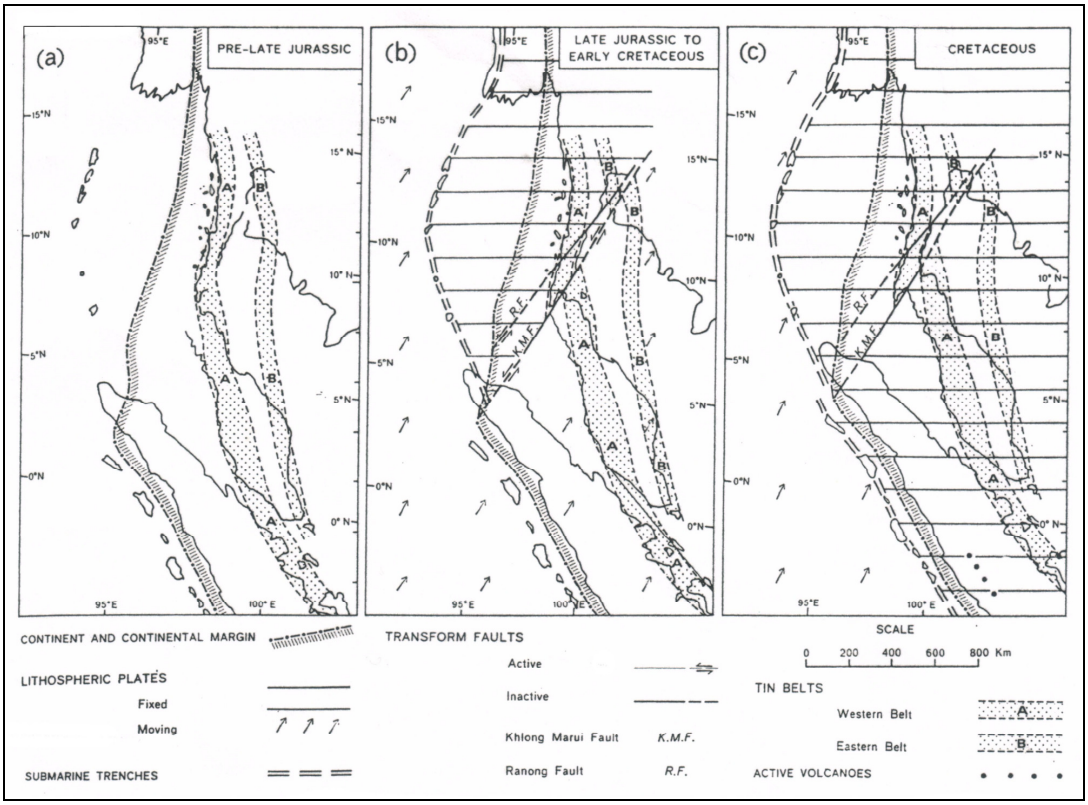

Figure 1.7. Relationship between ocean basin spreading coupled with the descent of the lithosphere and the fault movements in Thai peninsula in the late Mesozoic (Garson and Mitchell, 1975).

Earthquakes at fault zone

Earthquakes are natural phenomena that occur as a result of plate movement (Stein and Wysession, 2003). Plates normally move with friction at their

boundaries, causing stress and energy trapped inside. At a level where energy becomes excessive, it will be released in the form of an earthquake.

The plate movements create faults, which are fractures or deep cracks in the earth crust along which displacement occurs. Fault zones are parallel to each other and form a braided pattern it may vary in width ranging from a few meters to several kilometers. Faults are expanded through a series of minor movements due to stress in the crust and sudden release of energy. The displacement of faults ranges from a few centimeters to hundreds of kilometers. Faults rarely occur in a single rupture (Hamblin and Christiansen, 2001).

Thus, the major cause of earthquake is the stress originating in tectonic plate and faults that culminate in an earthquake. An earthquake virtually occurs on faults and if occurs on land close to the surface, it often leaves apparent ground breaking along the fault, for example, the earthquake that occurred in 1906 with magnitude 7.8 along the San Andreas Fault in San Francisco. The San Andreas Fault is the strike-slip fault which intersects California for a long distance (Figure 1.8).

Figure 1.8. The San Andreas Fault in the Carrizo Plain of California, the linear feature from upper left to lower right. A river is offset by this fault (Stein and Wysession, 2003).

Reid (1910) proposed the elastic rebound theory of earthquake on a fault. From his postulation, materials at distance on opposite side of the fault move relative to each other, but friction force maintains its position and prevents the side from slipping. Finally, the stress accumulated in the rock is beyond the limit the rock fault can withstand, and the fault slips, resulting in an earthquake.

1.1.3 Historical earthquakes in Andaman Sea and Thai Peninsula

In the historical records there is one earthquake reported for the Thai Peninsula. The location was near Ranong Fault Zone, probably in Myanmar near the border to Thailand, and it occurred on September 30, 1978 with 5.6 magnitude (Nutalaya, 1994, Figure 1.9).

However, earthquakes are more frequent in western and northern part of Thailand (see Figure 1.9). They are the northwards extension of the earthquake along the Sunda Subduction Zone and the faults zone in the Andaman Basin. Here earthquake occur quite often, especially also with higher magnitudes (see Figure 1.9, DMR, 1999).

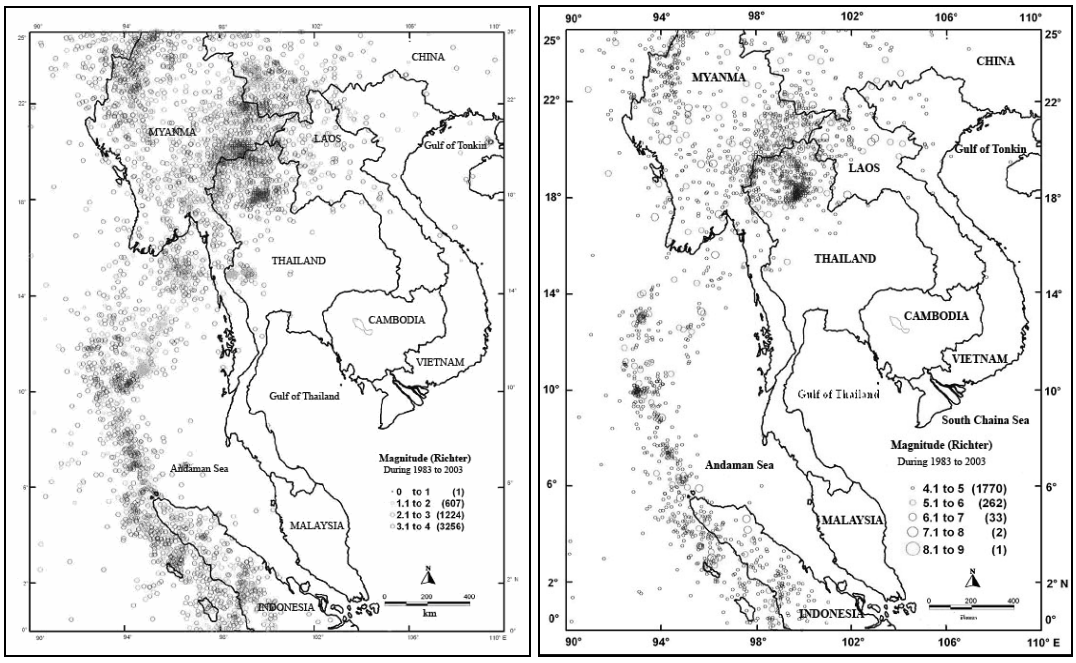

(a) (b)

Figure 1.9. Record of earthquakes in Thailand: from 1983 to 2003 with magnitude on Richter scale (a) magnitude 0 to 4 (b) magnitude 4 to 9 (DMR, 1999).

1.1.4 Earthquake measurement at Fault Zone

Recording equipment

The equipment used for measuring seismic events is known as seismometers, which are of different types as following (Trnkoczy et al., 2002a)

1. Short-period seismometers (SP) are used for measuring seismic events that have higher frequencies (0.1-100 Hz, with a corner frequency of 1 Hz). It is suitable for body wave measurements.
2. Long-period seismometers (LP) are used for measuring events that have lower frequencies. Practically, SP and LP are operated in conjunction for complete the seismic signal data.
3. Broadband seismometers (BB) provide more complete seismic information from about 0.01 to 50 Hz and allow a much broader range of seismic wave recording than the SP type.
4. Very broad brand seismometers (VBB) are capable of resolving the lowest frequency resulting from tidal currents and free oscillations of the Earth. The primary utility is for the research into greater depths of the earth, with the ability to record frequencies around and below 0.001 Hz (Asch, 2002).

The selection of equipment to be used for measuring the seismic event at fault zones depend upon many factors associated with the measurement, e.g., objective, time period, site, expenditure, etc. To measure for a short period of time and for local events, SP is more suitable while measuring for long periods, BB and VBB are better choices (Trnkoczy et al., 2002b).

Short period seismometer

A short-period seismometer (SP) is a velocity sensor for detecting motion where a coil moves in the permanent magnetic field and exert force in electromagnetic form. The motion induces a voltage in the coil; the current flowing in the coil produces a force and damps the mechanical free oscillation of a passive seismic sensor. The seismic signals are recorded by a seismograph (Trnkoczy et al., 2002a), Figures 1.10 and 1.11).

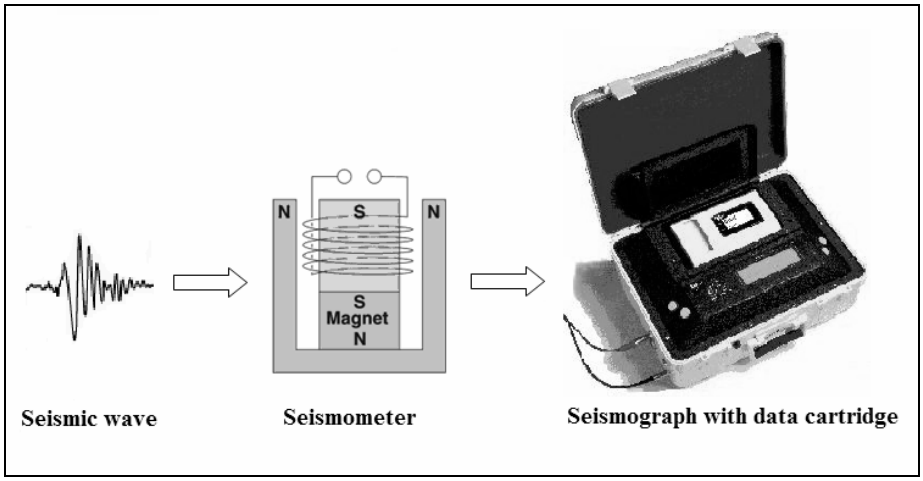

Figure 1.10. The seismic wave as ground displacement arrives at the velocity sensor, which then transfers the signal to a seismograph and stores it into a data cartridge in form of a digital data file.

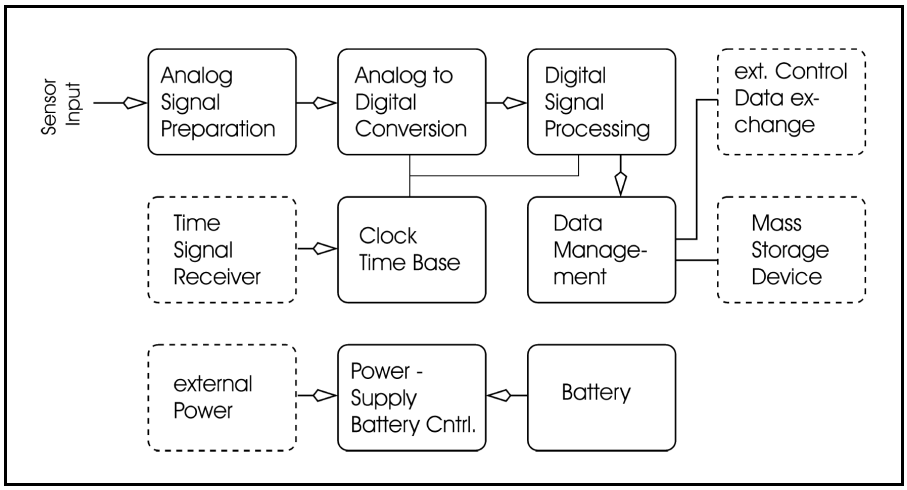

Figure 1.11. Seismic recording diagram in which the seismic analog signal is converted to a seismic digital signal with timing by the time signal receiver and power supply from battery or external power (Asch, 2002)

The short period seismometer measures the signal approximately between 0.1 to 100 Hz, with a corner frequency at 1 Hz. It provides a flat response to ground velocity for frequencies greater than the corner frequency (Figure 1.12).

Typical examples are the Kinemetrics SS-1, Geotech S13, and Mark Products L-4C. The 4.5-Hz exploration-type geophone is categorized in this group. This sensor provides reasonably good signals down to about 0.3 Hz at a fraction of the cost of 1.0-Hz sensor.

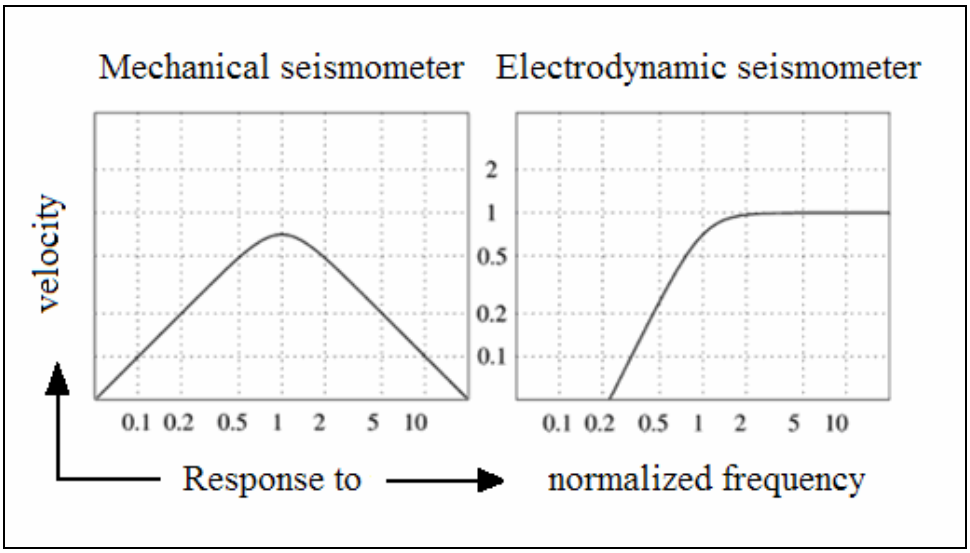

Figure 1.12. Response curves of a mechanical seismometer (spring pendulum, left) and an electrodynamic seismometer (geophone, right) of velocity input signal. The normalized frequency is the signal frequency divided by the Eigenfrequency (corner frequency) of the seismometer. The response curve has a second-order corner at the normalized frequency 1 (Wielandt, 2002).

Poles and zeros

The frequency response function of a seismometer is similar to a RC filter and standard inertial seismometer. The response function for the RC low pass filter is:

$$T_{RC}(\omega) = \frac{1}{1 + i\omega RC}$$

The amplitude frequency response function for a mechanical seismometer is:

$$T_d(\omega) = \frac{\omega^2}{\omega_0^2 - \omega^2 + i2\omega\omega_0 h}$$

where h is the damping coefficient (see Havskov and Alguacil, 2004)

The response function is any complex function .It is apparent that T (ω) for all systems made from discrete mechanical or electrical components (mass spring, coil, capacitor, semiconductor, etc., are represented by rational functions of iω, for example:

$$T(\omega) = \frac{a_0 + a_1(i\omega) + a_2(i\omega)^2 + ...}{b_0 + b_1(i\omega) + b_2(i\omega)^2 + ...}$$

where a_i and b_i are constants and the number of terms in polynomials depends on complexity of the system. The mechanical seismometer response can also be represented as:

$$T_d(\omega) = \frac{-(i\omega)^2}{\omega_0^2 + 2i\omega\omega_0 h + (i\omega)^2}$$

For a seismometer $a_0 = 0$, $a_1 = 0$, $a_2 = -1$, $b_0 = \omega_0^2$, $b_1 = \omega_0 h$, and $b_2 = 1$.That is a traditional way of giving response in SEED format.

$$T(\omega) = c\frac{(i\omega - z_1)(i\omega - z_2)(i\omega - z_3)....}{(i\omega - p_1)(i\omega - p_2)(i\omega - p_3)....}$$

where c is combined normalization constant for nominator and denominator polynomials, z is the zero (or root) of the nominator polynomials while the zero of the nominator polynomial is p whereas T (ω) is termed pole and zero.

Pole and zero are parts of the response data. The normalized response was calculated from the pole and zero data. At the frequency 1 Hz, normalized

response is 1 (normal). If the normalized response differs from 1 at1 Hz, it indicates the instrument is inaccurately functioning causing error in the amplitude.

Site selection

The capacity of seismic stations depends on the signal and noise characteristics of the site. The considered factors usually for site selection are as follows (Trnkoczy et al., 2002b).

(1) Geographical area under study: Delineation of major geologic faults on a geological map and assessment of the tectonic activity in that area.
(2) Seismo-geological information: These include underground conditions that reflect acoustic impedance; higher acoustic impedance, cause lower seismic noise.
(3) Topographic map consideration: On a hard rock or bed rock. The appropriate condition of the site is non-steep mountain slope, deep valley, mountain peak since there can be greater disturbances from seismic noise caused by wind, lightning strikes and icing to the equipments.
(4) Access to the station: The seismic stations are generally located in remote areas, away from human settlements but with reliable power supply.
(5) Recordability of seismic noise: The seismic noises are usually recorded in field measurements. Two sources of noise can be perceived, i.e., human activities and natural sources.
(6) Seismic data transmission and power supply.
(7) Land ownership and future land use.
(8) Climate conditions.

Trnkoczy et al. (2002b) suggest that a good way to begin with the site selection is to study topographic maps and gather information about potential sites, then comparing a few potential sites and choosing the best station at last.

Seismic noise

The recorded seismic signals may include events and noises. Noise is normally generated from (1) instrument (2) environmental perturbations, natural events and anthropogenic causes. The seismic noises are recorded in the noise power density acceleration spectrum in dB $(m/s^2)^2$/Hz unit (Bormann, 2002a).

Figure 1.13 illustrates the Peterson curves. It is the global high noise model (NHNM) and low noise model (NLNM). That the curves represent upper and lower bounds of a cumulative compilation of representative ground acceleration power spectral densities determined for noisy and quiet periods at 75 worldwide distributed digital stations, see Figure 1.13.

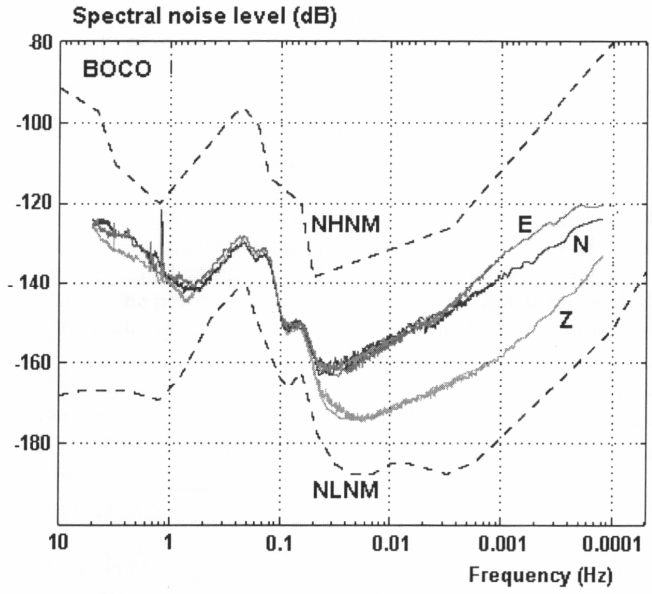

Figure 1.13. Peterson noise curves and noise spectra level for the IRIS station BOCO. Dashed lines represent the high-noise and low-noise model and the noise spectra in the 3 components (from Haskov and Alguacil, 2004).

Noises can be from natural as well as manmade origins. The population around the site and their activities surrounding the station, animals, agricultural and other activities nearby, for instances, blasting from mine, construction site, etc. are the causes of noises that interrupt the earthquake signals (Trnkoczy et al., 2002b).

1.1.5 Fault types

A fault is virtually a fracture or a deep crack in the earth crust along which displacement occurs. Fault is widened by a series of subsidiary movement that occur following stress in the crust with abrupt release of energy, culminating in an earthquake. The displacement along faults ranges from a few centimeters to hundreds of kilometers (Hamblin and Christensen, 2001). In most cases, a fault is created by a series of ruptures rather by a single one. Fault zone are located parallel to each other or form a braided pattern. Fault zones are variable in width, ranging from a meter to several kilometers (Keller, 2000).

An **active fault** is the one that demonstrates movement during the past 10,000 years (Holocene Epoch). Fault with displacement occurred during the Pleistocene Epoch of Quaternary Period (about 1.65 million to 10,000 years ago) but not in the Holocene is classified as **potentially active faults** and the fault which have not moved during the past 1.65 million years classified as **inactive fault** (Keller, 2000).

There are three types of faults (Drury, 1993; Bormann et al., 2002c):

Normal faults are usually the result of extensional stress where the faults moved vertically, while the rock above the fault plane (hanging wall) moved downward in relation to those beneath the fault plane (foot wall, see Figure 1.14). Normal faults dominate the oceanic ridges, the continental rift systems, and the rifted continental margins.

Reverse faults are those with vertical displacement where the hanging wall moves up over the foot wall, see Figure 1.15. Low-angle reverse faults are known as thrust faults. Reverse faults are the result of horizontal compression with the maximum stress perpendicular to the trend of the fault. It shortens and thickens the crust.

Strike-slip faults are high-angle fractures in which slip is horizontal, parallel to the strike of the fault plane (Figure 1.16). There is little or no movement in vertical direction. Strike-slip faults are the result of lateral slip.

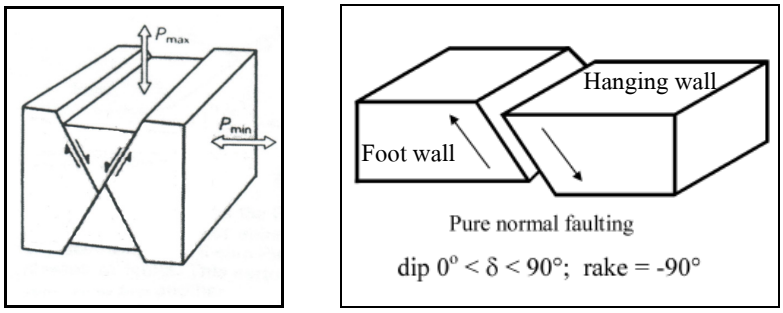

(a) (b)

Figure 1.14. (a) Normal faults with larger stress in vertical component than in horizontal one, (b) the hanging wall moves downward while the foot wall moves up (Drury, 1993; Bormann et al., 2002c).

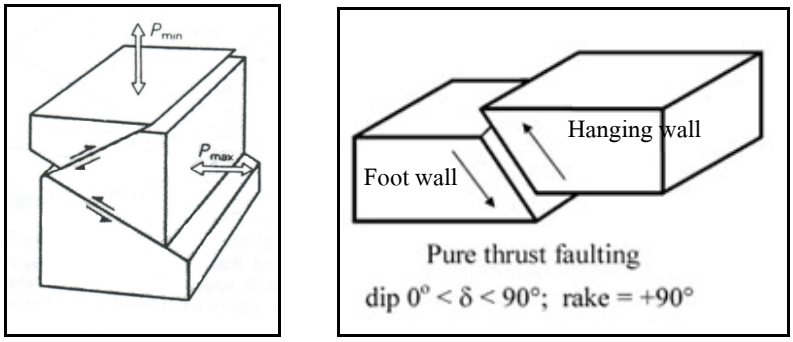

(a) (b)

Figure 1.15. (a) Reverse faults with greater stress in horizontal component than in vertical counterpart, (b) hanging wall moves up and/or the foot wall moves down (Drury, 1993; Bormann et al., 2002c).

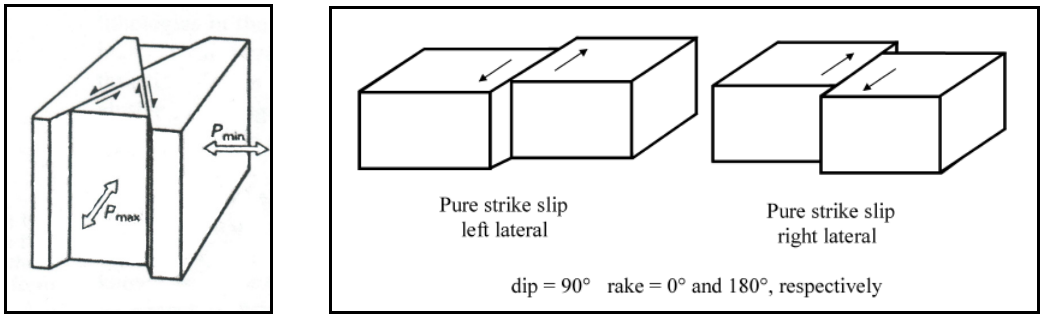

(a) (b)

Figure 1.16. (a) Strike-slip faults with stress in horizontal component, (b) blocks move in horizontal direction with strike slip motion (Drury, 1993; Bormann et al., 2002c).

1.1.6 Earthquake measurements at fault zone

For seismological fault zone studies, the objectives of the measurements have to be clear regarding parameters to be measured, period of measurement, equipment, station site, etc. The possible objective of measurements could be to determine the scale of earthquakes at a fault zone. In measuring for a short time (temporary), a short-period seismometer is more suitable while measuring for a long period, broadband seismometer is advantageous. After measurement planning for time and equipment, the next step is selecting the site for a recording station and setting up seismic stations. At a fault zone, the seismic stations have to be set up over the fault zone in order to minimize the discrepancy in earthquake location. The epicenter (location of earthquake on the surface) can be detected from at least 3 seismic stations. If five or even more seismic stations exist, the focal mechanism can be elaborated (Trnkoczy et al., 2002a).

After shock study

An aftershock occurs in close proximity of a massive earthquake event as the stresses in the plate are continuously released (Trnkoczy et al., 2002b) In such a case, a seismic network is preferable set up in a region where the main shock, respectively main earthquake, occurred in order to monitor the aftershocks. The Landers Earthquake is an example for that (Scholz, 2002).

The Landers earthquake occurred on June 28, 1992 with a magnitude 7.3 (Mw = 7.3). It occurred over a system of strike-slip faults along the western margin of the California Shear Zone (Figure 1.17). The sequence began on April 23, 1992; with magnitude 6.1 Joshua Tree Earthquake. It produced a north striking aftershock sequence that extended about 20 km north from epicenter. The main shock occurred two months later, propagating unilaterally 60 km northwest and ruptured at least five faults in an echelon array. The after shock series of magnitude more than 5 expanded the rupture to the southeast in the vicinity of the Joshua Tree aftershock zone. From a minor maximum near the hypocenter, the displacement was enlarged northward to a maximum of 6 m at the overlap between the Homestead Valley and Camp/Emerson faults. Slip moved between the extensional jogs, separating the three

main faults evidently formed as a result of stress transfer with connection between them. In the 6x3 km^2 overlap region of the Johnson Valley and Homestead Valley faults, surface slip gradually diminished toward the ends of both faults and 1-2 m slip was transferred by a previously unrecognized linking cross-fault (Scholz, 2002).

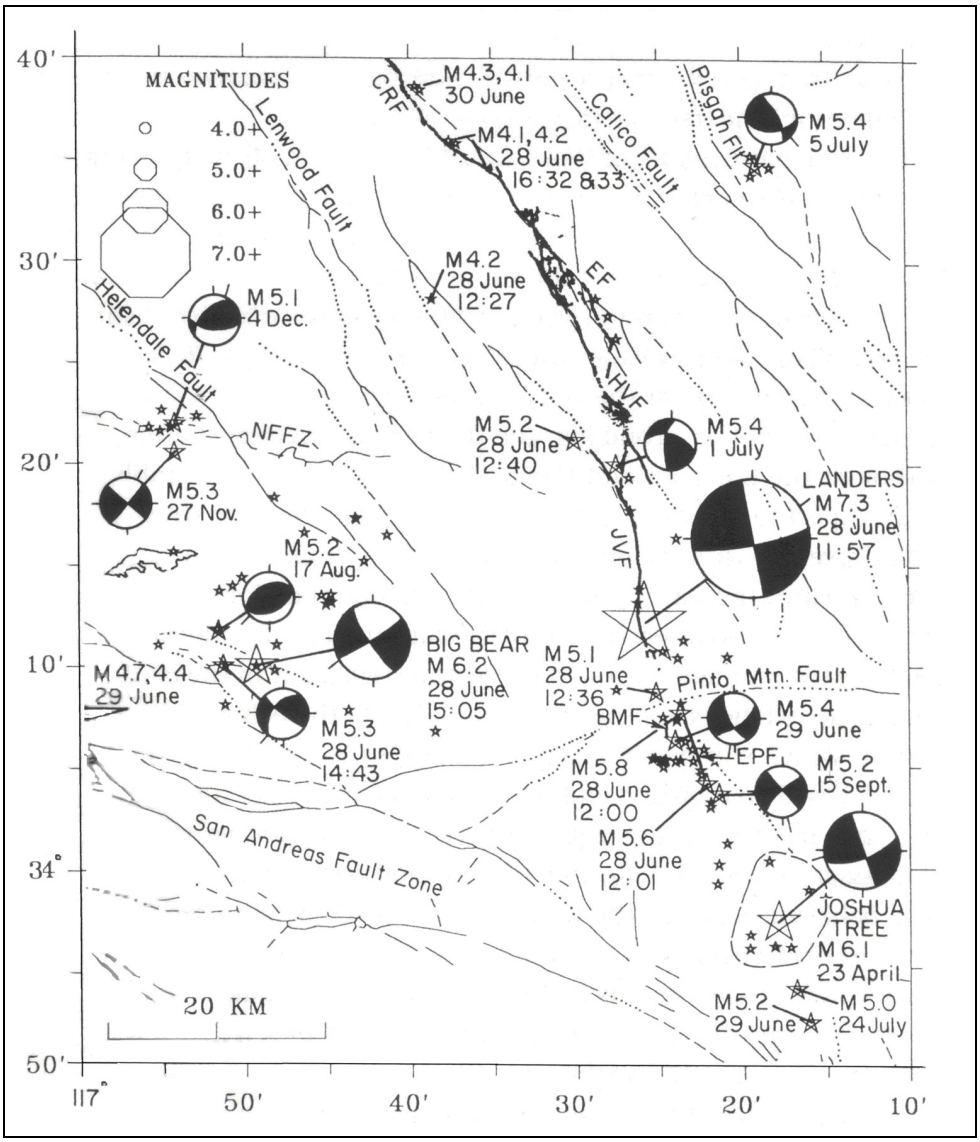

Figure 1.17. Locations and magnitudes of the Lander earthquake sequence with M = 7.3 main shock and aftershock on fault zone. All earthquakes are recorded from April to December, 1992. The dark lines represent surface rupture due to the main shock (from Scholz, 2002).

1.1.7 Velocity model

During an earthquake, the seismic elastic waves propagate through the earth. There are two major seismic waves, i.e., body wave and surface wave (divided from criterion of ray path). The body wave is constituted by compressional waves (P-wave) and shear wave (S-wave). The P-wave is of greater velocity than S-wave and propagates in the same direction of the oscillating particles. Direction of S-wave is perpendicular to the direction of oscillating particle and the wave can not propagate through the liquid medium (Figure 1.18 a). The surface waves propagate on the surface around the earth. There are two types of surface wave, i.e., Love waves (LQ or G) and Rayleigh waves (LR or R). The propagation of surface wave is illustrated in Figure 1.18 b.

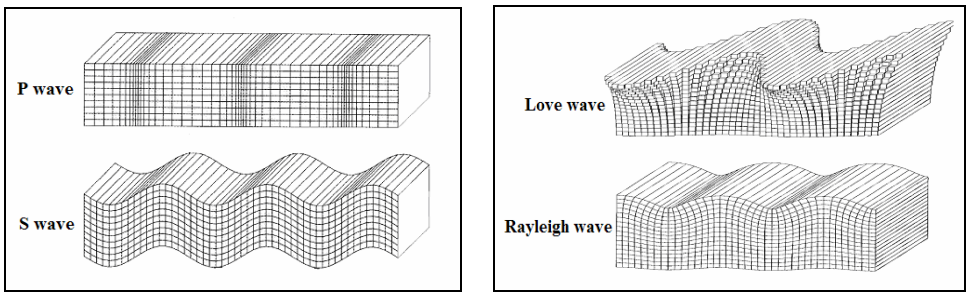

(a) (b)

Figure 1.18. Seismic waves propagate in a homogeneous medium with the direction from left to right, (a) displacement from a harmonic P-wave (top) and S-wave (bottom), (b) displacement from the horizontal propagation of Love wave (top) and Rayleigh wave (bottom) (Shearer, 1999).

With Pg, Sg is the primary and secondary wave phase in the granitic layer of the earth crust. P* and S* are the primary and secondary wave phase that are refracted at an intermediate discontinuity; Pn, Sn is the primary and secondary wave phase travelling along the Moho discontinuity (Bormann et al., 2002a, Figure 1.19).

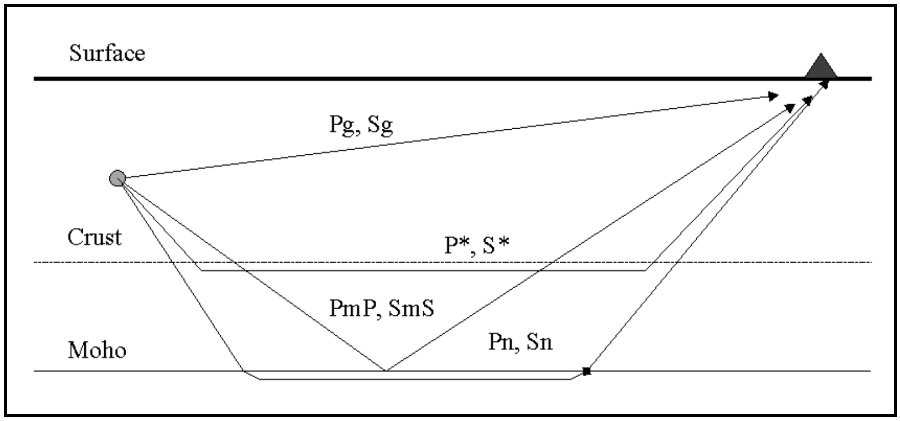

Figure 1.19. A simplified model of the ray path in the main crustal that Pg, Sg are the direct P wave and S wave. P* and S* are P wave and S wave that are refracted at an intermediate discontinuity. PmP, SmS are the P wave and S wave that are reflected at the upper mantle (Moho). Pn and Sn are the P wave and S wave that are refracted at upper mantle (Bormann et al., 2002a).

Following an earthquake, time and location are determined. The velocity model is important for the determination of earthquake location and origin time (Bormann et al., 2002b). The IASP91, AK135 and Jeffrey and Bullen travel timetable are samples of 1-D global velocity models.

IASP91 Model (Kennett and Engdahl, 1991)

The *IASP91* are seismological tables prepared for a wide range of P and S waves. There are two crustal layers with P_1 velocity 5.80 km/s, S_1 velocity 3.36 km/s with a depth of 20 km. Conrad Discontinuity marks the boundary to the second layer, with P_2 velocity of 6.5 km/s, S_2 velocity of 3.75 km/s and a depth at 35 km. The Upper Mantle layer has a P_3 velocity of 8.04 km/s and a S_3 velocity of 4.47 km/s (see Table 1.1, Bormann, 2002c).

AK135 Model (Kennett, 2005)

The *AK135* tables are the updated version of *IASP91* for matching the behavior of a wider range of phases. The *AK135* model was described by Kennett (2005), Kennett and Engdahl (1991) and was based on new empirical travel time tables using the *IASP91* model (relocating events). The *AK135* is a radial stratified velocity model and the travel time tables are derived from the model so that a consistent basis exists for all phases. The P wave travel times are similar to *IASP91,* but with significant changes in the S wave and especially the core phases. The crust layer has a P_1 velocity of 5.80 km/s, an S_1 velocity of 3.46 km/s with a depth at 20 km, the Conrad Discontinuity. Layer 2 has a P_2 velocity of 6.5 km/s and a S_2 velocity of 3.85 km/s with a depth at 35 km, the Moho Discontinuity. The Upper Mantle layer has a P_3 velocity of 8.04 km/s and a S_3 velocity of 4.49 km/s (see Table 1.1., Bormann, 2002c).

Jeffreys and Bullen Model (Jeffrey and Bullen, 1967)

Jeffreys and Bullen travel time tables provide major wave phases. They have two crustal layers, where layer1 has a P_1 velocity of 5.56 km/s and a S_1 velocity of 3.36 km/s with a depth at 15.73 km, the Conrad Discontinuity. Layer 2 has a P_2 velocity of 6.49 km/s and a S_2 velocity of 3.74 km/s with a depth at 33.6 km depth, the Moho Discontinuity. The Upper Mantle layer has a P_3 velocity of 7.79 km/s and a S_3 velocity of 4.42 km/s (Table 1.1, Jeffrey and Bullen, 1967).

Table 1.1. Velocity and depth data for the 1-D Earth models IASP91 (Kennett and Engdahl, 1991), AK135 (Kennett, 2005), and Jeffreys and Bullen (Jeffrey and Bullen, 1967).

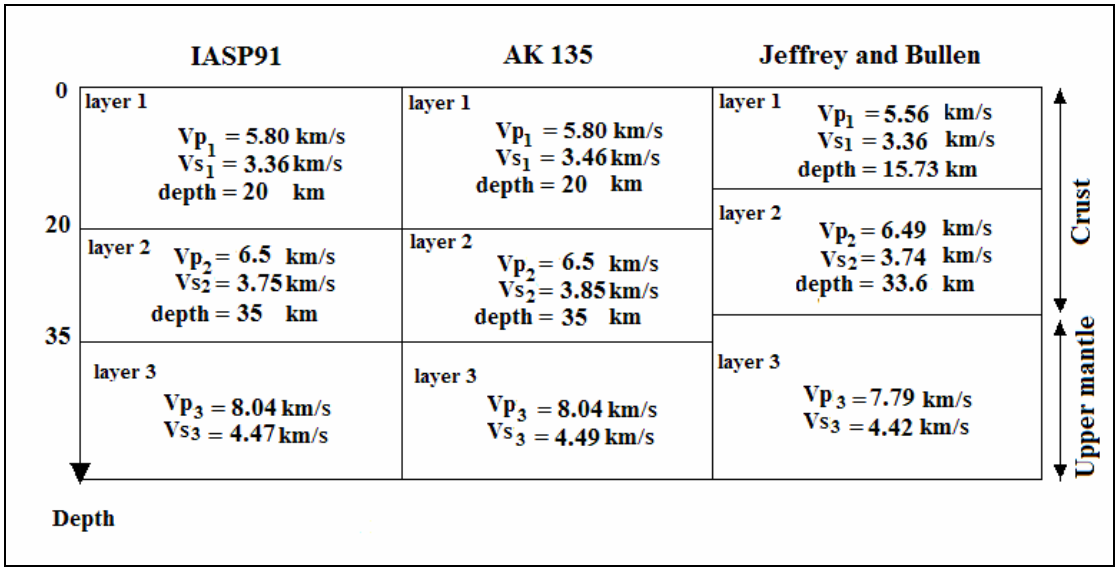

1.1.8 Earthquake location determination

The earthquake location is identified by its hypocenter (x_0, y_0, z_0) with x_0 is longitude, y_0 is latitude, and z_0 is depth below surface (km) and t_0 is the origin time, the start time of the earthquake rupture (Havskov, 2002). The earthquake epicenter is the projection of hypocenter on the earth surface (x_0, y_0). The procedure to determine epicenter is as follows:

Multiple station location

The epicenters are determined using the difference between the S and P arrival times from at least 3 different seismic stations. The epicenter is located from circles with the center at the stations and the radii equal to the epicenter distances calculated from the S-P time (delta time, Δt). The circle crosses at one point or otherwise the chords are drawn over the crossing point (Figure 1.19 a, b). S1, S2, S3 are the stations with epicenter distance, radii, d1, d2, d3, respectively.

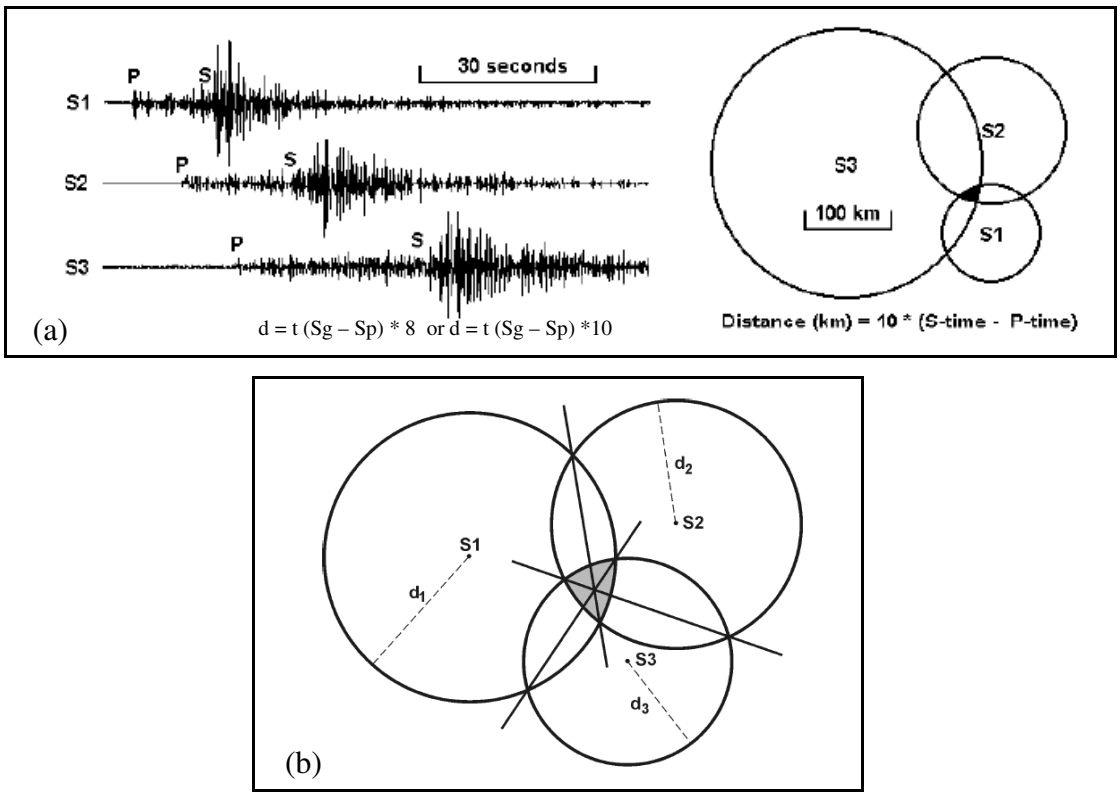

Figure 1.20. (a) P and S wave arrival time picking (P, S) in each seismogram (S1, S2, S3) from each station and used for delta time calculation. (b) Location of epicenter with epicenter distances d1, d2, d3 from Station S1, S2, S3, respectively (Bormann and Wylegalla, 2002a).

Single station location

At any seismic station it is possible to determine the earthquake location (epicenter) using the three-component data, north (N), east (E) and vertical (Z) component. The vector of the P- wave motion can be used to calculate the back azimuth to the epicenter. The ratio of amplitude A_E/A_N on the horizontal component is used to calculate the azimuth: AZI (Bormann and Wylegalla, 2002b) with:

$$AZI = \arctan A_E/A_N$$

The first polarity used to obtain the back azimuth. With 3 components the epicenter can be located (Figure 1.20). However, as other factors on the travel

path of the wave can influence its amplitudes this methods has limitations (Bormann et al., 2002c).

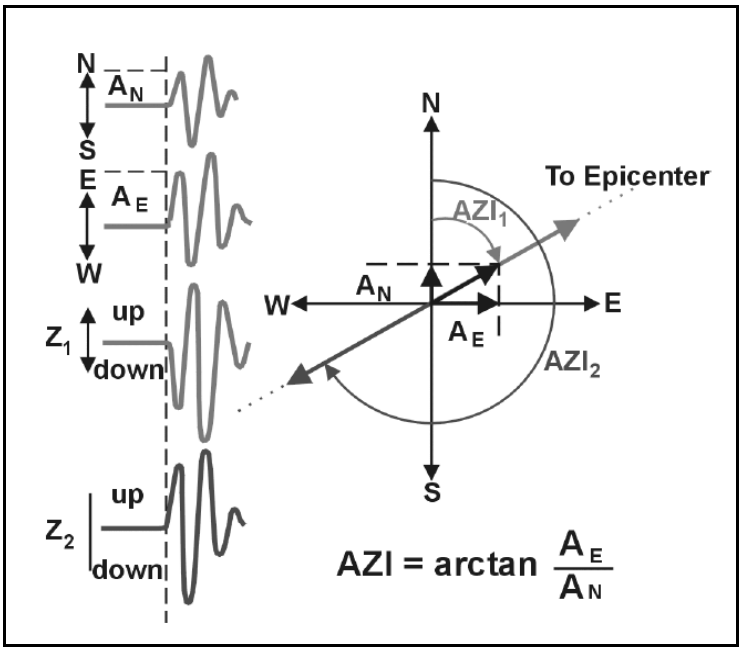

Figure 1.21. P-wave first motion in 3-component record (left) and (back) azimuth AZI to the epicenter (right), from Bormann and Wylegalla, 2002b.

1.1.9 Uncertainty in earthquake location

The determination of an earthquake location is subject to uncertainty due to many factors (Trnkoczy et al., 2002a). The main factors are:

(1) Error from P and S wave arrival time picking. The epicenter distance changes if P-wave and S-wave arrival time varies (Figure 1.21).

(2) If the distance between seismic stations are relatively close and the earthquake epicenter is outside the station area, then the circles in the circle and chord method do not cross in a point rather than in an area, giving the location a higher uncertainty (see Figure 1.22).

(3) If the velocity model of that area is inappropriate the location will have an uncertainty as the distance determination is based on the travel time data from the velocity model.

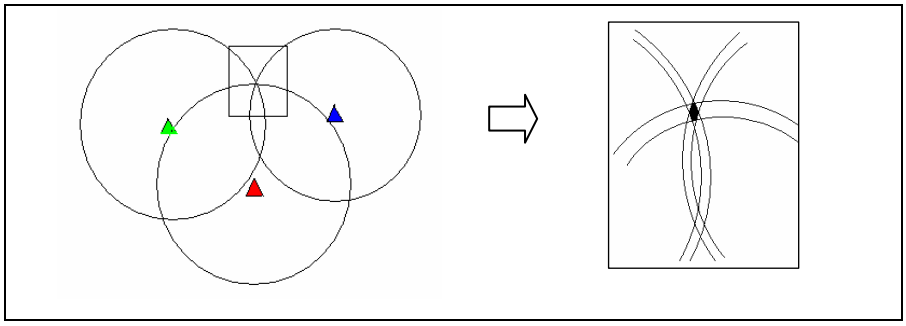

Figure 1.22. Earthquake epicenter determination with circle and chord method (left), and an uncertainty of the earthquake location from P and S wave picking (right).

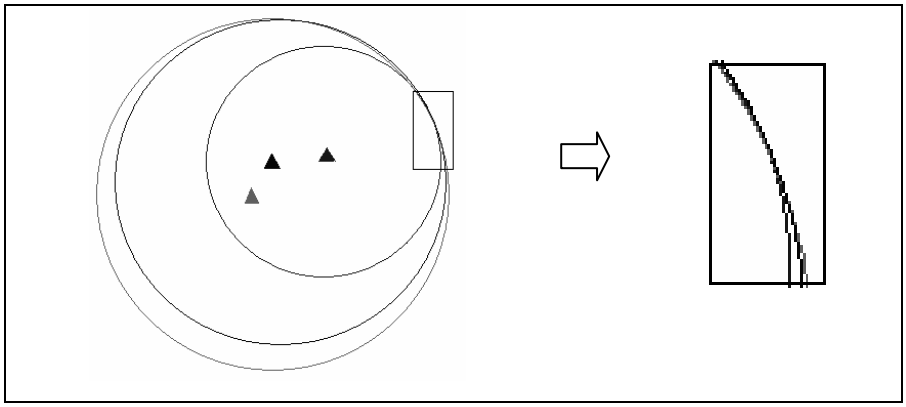

Figure 1.23. The uncertainty of an earthquake location using data of recording stations in close proximity (left). The crossed circles do not provide a clear epicenter location, rather then an area (right).

1.1.10 Local magnitude determination

Richter scale

The magnitude of an earthquake provides the scale of the size of an earthquake (Richter, 1935). Many scales of earthquake magnitudes exist although the original one is the Richter scale developed in 1935 by Charles F. Richter for southern California earthquakes (Richter, 1935). It is the local magnitude, Ml, which has short epicenter distance of less than 6 degrees. The magnitude of an earthquake is determined from the logarithm of the amplitude of the waves recorded by a Wood-

Anderson seismograph (amplitude with magnification, not real ground displacement). The Wood-Anderson Seismograph has a natural period of T_S = 0.8 s with a damping factor D_S = 0.8 (Richter, 1935), and with a magnification of 2080±60 (Uhrhammer et al., 1996). The formula for calculating the local magnitude is:

$$Ml = \log A_{max} - \log A_0 \quad (1)$$

where A_{max} is amplitude sum in mm, measuring zero to peak in horizontal component (east-north component, $A_{max} = \sqrt{(E^2_{max} + N^2_{max})}$) of Wood-Anderson seismograms and $-\log A_0$ is the correction or attenuation value.

Hutton and Boore (1987) proposed following correction value for earthquakes in Southern California:

$$-\log A_0 = 1.110 \log (R/100) + 0.00189 (R- 100) + 3 \quad (2)$$

where R is the hypocentral distance in km, $R = \sqrt{(\Delta^2 + h^2)}$, Δ is the epicentral distance in km, h is hypocenter depth in km. Thus the local magnitude for these earthquakes is

$$Ml = \log A_{max} + 1.110 \log (R/100) + 0.00189 (R- 100) + 3 \quad (3)$$

where A_{max} is the amplitude sum in mm, on a seismogram from a Wood-Anderson Seismograph, measuring zero to peak in horizontal components (East and North component). R is the hypocentral distance in km.

Minus Magnitude

The Richter scale (local magnitude Ml) is a numerical figure that quantifies the size of an earthquake. It is in a logarithmic scale calculated from logarithm of the combined maximum amplitudes of the shear waves in horizontal

component (the largest displacement from zero on a seismometer output) with the records from a Wood-Anderson seismograph. A magnitude 0 on the Richter scale (Ml = 0) is an earthquake that has a maximum combined horizontal displacement of 1 micrometer on a seismogram recorded on Wood-Anderson seismometer at 100 km from the epicenter of that earthquake. It is formatted to preclude negative magnitudes, modern seismometers. However, modern seismometers have higher resolution, so they can measure earthquake amplitudes at much smaller scale (nanometers). If the amplitude at 100 km is below 1 micrometer, the local magnitude becomes lower than zero (as $\log_{10}$ of a number less than 1 is negative). Currently the routine recording of earthquakes can determine local magnitude both with positive and negative values (Joswig, 2007).

1.1.11 Man-made event

A seismograph also can record seismic events that occur anthropogenically, for examples activities like blasting, nuclear explosion, vibrations. These events are often near surface seismic events that can generate short-period fundamental-mode Rayleigh waves (Rg). Rg waves represent normal dispersion and have relatively large amplitudes on the vertical component. This is not seen by seismic events deeper than about one wavelength and hence Rg waves can be used to separate between man-made near surface events and natural earthquake events with a depth between 5 and 25 km or deeper. The Rg wave experiences stronger attenuation than Lg wave (Love wave); see Bormann et al. (2002a).

Figure 1.23 shows wave forms recorded after a mining rock burst in Saarbrücken, Germany, with Ml=3.7, at 80 km epicenter distance and 1 km depth. The recording station was in Luxemburg (Bormann et al., 2002a). This event produced Rg waves, which can be seen on the vertical z-component.

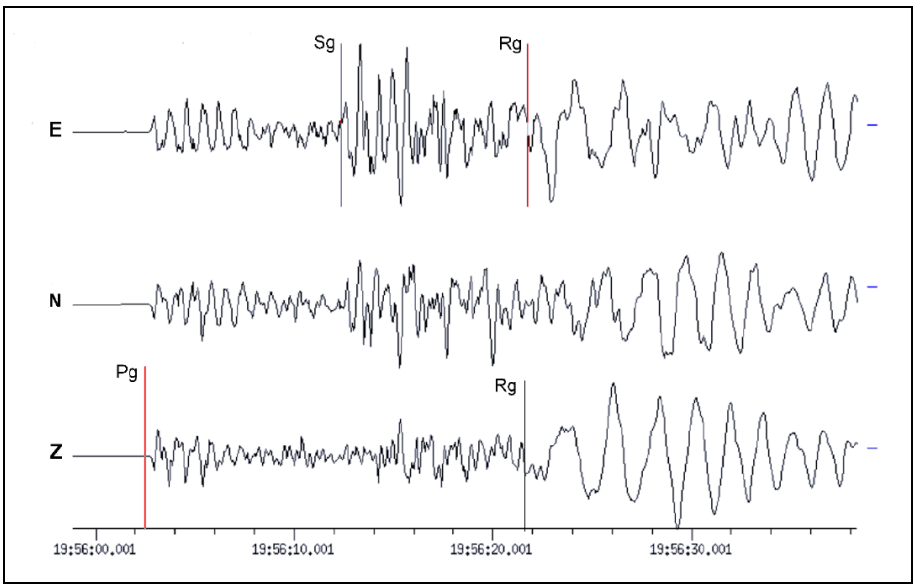

Figure 1.24. Seismogram from a mining rock burst in Saarbrucken, Germany, recorded at station WLF in Luxemburg (D = 80 km, h = 1 km, Ml = 3.7). On the E and vertical Z-components Rg waves with higher amplitudes than the S waves can be seen (Bormann et al., 2002a).

1.2 Objectives

The Mw 9.3 earthquake on the 26 December 2004 triggered a tsunami with devastating effects on the coastlines along the Indian Ocean, including the Andaman beaches in Southern Thailand.

However, shortly after this disaster there was concern among the people and responsible government agencies, that the 26 December 2004 Earthquake might have resulted in the (re)activation of the Ranong and Khlong Marui Fault Zones in Southern Thailand, as consequent local earthquakes might have effects on the infrastructure and the people there. Prior, both fault zones were identified as dormant.

Therefore, the objective of this study was to set up a seismic network of short period seismometers in Southern Thailand to monitor possible earthquakes along the Ranong and Khlong Marui Fault Zones, to analyze the seismograms and to determine the locations, magnitudes and origin times of the recorded earthquakes.